Journal of Molecular Liquids 399 (2024) 124326

Contents lists available at ScienceDirect

Journal of Molecular Liquids

journal homepage: www.elsevier.com/locate/molliq

Deciphering the structure of deep eutectic solvents: A computational study from the solute's viewpoint

Chiara Sepali [a], Sulejman Skoko [a], Luca Guglielmero [a], Tommaso Giovannini [a], Andrea Mezzetta [b], Felicia D'Andrea [b], Christian Silvio Pomelli [b], Lorenzo Guazzelli [b,*], Chiara Cappelli [a,c,**]

[a] Scuola Normale Superiore, Classe di Scienze, Piazza dei Cavalieri 7, 56126 Pisa, Italy
[b] Dipartimento di Farmacia, Università di Pisa, Via Bonanno 6, 56126 Pisa, Italy
[c] Consorzio Interuniversitario Nazionale per la Scienza e Tecnologia dei Materiali (INSTM), UdR Pisa-SNS, Piazza dei Cavalieri 7, 56126 Pisa, Italy

ARTICLE INFO

Keywords:
UV absorption spectra
Deep eutectic solvents
Molecular dynamics
HMF
QM/MM

ABSTRACT

In the last few years, Deep Eutectic Solvents (DESs) have emerged as sustainable alternatives to traditional organic solvents. The high degree of freedom when tailoring DES structures represents, at the same time, their most praised and most complicated feature. Indeed, given the enormous number of possible combinations, the selection of the most suitable DES for a given application cannot be based on a trial-and-error approach; therefore, reliable computational tools are needed to fully exploit DESs potentialities. In this work, we propose the first computational protocol to investigate absorption properties of solutes dissolved in DES. The protocol combines an accurate sampling of the solute-solvent phase-space by means of Molecular Dynamics (MD) and a fully atomistic Quantum Mechanics/Molecular Mechanics (QM/MM) approach to describe intermolecular interactions and spectral properties. In this way, specific interactions such as hydrogen bonding, which characterize DES complex interaction patterns, are properly modelled. The robustness and reliability of the method are proved by comparing computed data with experimental spectra of 2-hydroxymethylfurfural and syringic, vanillic, *p*-coumaric, gallic, and caffeic acids dissolved in DES and water. These molecules have been chosen because of their relevance in the frame of biomass valorization. Remarkably, the protocol allows getting insights into DES/water mixtures and opens up to the prediction of aqueous DES behaviour of the water threshold which causes the switch from water-in-DES to aqueous electrolyte-like environments.

1. Introduction

In the last few decades, there has been an increasing interest in the research of green alternatives to conventional organic solvents. [1,2] With the first paper on the subject published in 2001, [3] deep eutectic solvents (DESs) are a relatively new class of solvents that is gaining increasing attention in recent years. DESs consist of a mixture of two or more components that act as hydrogen bond donors (HBDs) and hydrogen bond acceptors (HBAs), typically salts, which displays a melting temperature at the eutectic composition much lower than the melting temperature expected for an ideal eutectic behaviour. [4–7] The hydrogen bond network characterizing DESs gives rise to a set of intriguing physicochemical properties, [8–14] favourable to a plethora of different applications, such as synthesis and catalysis, [15–17] extraction processes, [18–21] biomass fractionation and valorization. [22–24] The possibility of preparing completely natural-based DESs, characterized by low toxicity, [25] together with their easy preparation not requiring any purification process, makes DESs ideal green solvents for chemical transformation, [15,26] biomass processing [27–30] and pharmaceutical uses. [31] DESs are designer solvents, which means that their properties may be tailored on the needs of a specific application. This is possible by selecting proper DES constituents, molar ratio, and even the amount of water added to the system, all parameters that strongly influence the structure and properties of DESs. While the possibility to customize the solvent is a great advantage over traditional organic solvents, the experimental trial-and-error tuning required for defining the

* Corresponding author at: Dipartimento di Farmacia, Università di Pisa, Via Bonanno 6, 56126 Pisa, Italy.
** Corresponding author at: Scuola Normale Superiore, Classe di Scienze, Piazza dei Cavalieri 7, 56126 Pisa, Italy.
E-mail addresses: lorenzo.guazzelli@unipi.it (L. Guazzelli), chiara.cappelli@sns.it (C. Cappelli).

https://doi.org/10.1016/j.molliq.2024.124326
Received 27 December 2023; Received in revised form 31 January 2024; Accepted 22 February 2024
Available online 28 February 2024

optimal system is time-consuming and costly, thus ultimately unattractive. [8]

Therefore, the transition from organic solvents-to-DESs asks for theoretical and computational studies focusing on DESs unique properties, [7,32–42] which can offer valuable insights into the interactions between molecules and DESs, and how the latter affect molecular properties and related processes. DESs are, in fact, well-known for the robust intermolecular interactions existing among their components, and with the solutes, [43] making DESs computational simulation particularly challenging. [7] For this reason, similarly to experimental procedures, current theoretical approaches need to be translated and validated for use in this novel context. Indeed, the best approach would be a synergistic experimental-theoretical investigation, potentially accelerating the transition toward the practical use of green solvents such as DES. This work focuses on the absorption properties of organic molecules dissolved in DES. Although the experimental recording of UV spectra of selected probes in DESs has been performed for quite some time aiming at determining the polarity of these systems, [44,45] through the solvatochromic parameters, theoretical studies are missing. To this end, we propose a computational protocol for modelling the absorption spectra of these systems, capturing the peculiar aspects of the solvation phenomenon and its effect on the solute spectral response. [46–56] Remarkably, the protocol is validated through close comparison with experimental spectra. To the best of our knowledge, this is the first work specifically dealing with DES solvation effects on spectroscopic signals of molecular systems.

Our protocol is defined within the multiscale, focused models framework, [50,57,58] in which the solute is described in all its degrees of freedom while treating the solvent at a lower level of theory. [59] In our method, the solvent is described employing fully atomistic classical molecular mechanics (MM) force fields, while the solute is described at the QM level (QM/MM). [59,60] For a physically consistent description of the solvation phenomenon, we employed the Discrete Reaction Field (DRF) model, [61,62] which accounts for solute-solvent mutual polarization, [49,50,63] by endowing each MM with a fixed charge and an induced dipole which simulate the polarization as a response to the QM electric field. It is worth remarking that a fully atomistic polarizable QM/MM approach is indeed the ideal choice to accurately reproduce the properties of a molecular system surrounded by a DES, considering the intricate HB patterns formed between its components and with the solute. Furthermore, to properly sample solute-solvent conformational phase space, our procedure involves coupling the polarizable QM/DRF model with a classical molecular dynamics (MD) simulation, which allowed us to describe the dynamical aspect of the solvation phenomenon. [50]

The protocol is exploited to simulate the absorption spectra of organic systems dissolved in both water and DES, in this case, choline chloride (ChCl) and ethylene glycol (EG) 1:3, which is one of the most widely HBA-HBD combinations used in the literature. [8,64,65] The proposed approach has been then expanded to consider water-DES mixtures at varying molar percentages of water. As mentioned previously, water is a critical player for DES systems. Indeed, it may have beneficial effects on the properties of the systems (often lowering the viscosity), and hence it is often intentionally added to the DES, or it may cause its de-structuring beyond a certain, yet often unknown, amount. Since the work by Edler et al., [66] a great deal of attention has been devoted to determining the effect of water on DESs, namely the transition from water-in-DES to DES-in-water to solution of DES components in water, often referred to as aqueous electrolyte-like solutions, a debate which is still ongoing. [67]

To validate our procedure, we focused on well-studied systems in DES, such as polyphenolic compounds (caffeic and *p*-coumaric acids – hydroxycinnamic acids – and vanillic, syringic, and gallic acids – hydroxybenzoic acids) and 2-hydroxymethylfurfural (HMF), of great importance for sustainable development. [63,68–84]

In the following section, the computational method is presented and the QM/DRF solvation model is briefly recalled. Then, an ample explanation of the experimental and computational details used to obtain the absorption spectra in DESs, water, and water-DES mixtures is reported. Subsequently, MD trajectories are discussed and analyzed to get information about the conformational aspects of the solutes and their interactions with the two solvents. Finally, the simulated absorption spectra are discussed and compared with experimental data, with a focus on the case of water-DES mixtures.

2. Computational methods

The computational protocol used for simulating the absorption properties of phenolic acids and HMF in water and DES is described in this section. The same procedure is also exploited to simulate the absorption spectra of vanillic acid in water-DES mixtures with three different molar percentages of water (25%, 50%, and 75%). The protocol that is exploited generalizes what has been developed by some of the present authors for aqueous solutions in Refs. 49 and 50. The protocol is composed of multiple steps. First (1), QM and MM regions have to be defined. In this study, the solute molecules, i.e., phenolic acids and HMF, are treated at the QM level, while the solvent composes the MM portion. The second step of protocol (2) is the sampling of the solute-solvent conformational phase-space, which is crucial to capture the dynamics of solvated systems and the conformational aspects of the solute. A static distribution of solvent molecules around the solute does not accurately reflect the dynamic nature of the solvation phenomenon, where the solvent molecules are constantly in motion. In this work, we exploit classical MD simulations. To accurately represent the system configurations and related energies, MD simulations are run for a few nanoseconds to sample the entire phase space. A set of uncorrelated structures is extracted from the resulting MD trajectories (3) and used for the subsequent QM/MM calculations of spectra (4). The extracted snapshots are cut into spherical droplets with a certain radius sufficiently large to consider all long-range solute-DES (water) interactions. Note that absorption spectra calculations are performed on the extracted structures without geometry optimization. In this way, both the conformational freedom of the solvent molecules surrounding the solute and the flexibility of the solute are taken into account. Moreover, the solute-solvent system is not assumed to be fully relaxed, thus providing a more accurate representation of the actual dynamics of the solution. [49] The total number of extracted snapshots is selected to ensure the convergence of the desired spectral signal. The resulting properties are averaged to generate the final spectra (5) and compared to experimental data.

In this study, the Discrete Reaction Field (DRF) model [61] is used to describe the solvent molecules in QM/MM calculations, due to the availability of parameters for the selected DES (choline chloride and ethylene glycol). This model offers an electrostatic description of the environment, where each solvent atom is associated with both a charge and a dipole. The charge of each atom is fixed, whereas the atomic dipole can vary as a response to the QM density and the other multipoles (fixed charges $\mathbf{q}$ and the induced dipoles $\boldsymbol{\mu}^{\mathrm{ind}}$). DRF is thus defined by two atomic parameters: the charge (q) and the polarizability (α). The QM/MM interaction energy is given by: [61]

$$E_{\mathrm{QM/MM}} = \mathbf{q}\mathbf{V}(\rho_{\mathrm{QM}}) - \frac{1}{2}\boldsymbol{\mu}^{\mathrm{ind}}(\rho_{\mathrm{QM}})\mathbf{E}(\rho_{\mathrm{QM}}) \tag{1}$$

where the QM/MM electrostatic interactions are written in terms of the MM multipoles interacting with the electrostatic potential $\mathbf{V}(\rho_{\mathrm{QM}})$ and field $\mathbf{E}(\rho_{QM})$ generated by the QM electronic and nuclear charge densities at each MM position. The induced atomic dipoles can be obtained by solving a linear system that minimizes the total energy of the QM/MM system: [61]

$$\mathbf{A}\boldsymbol{\mu}^{\mathrm{ind}}(\rho_{\mathrm{QM}}) = \mathbf{E}(\rho_{\mathrm{QM}}) \tag{2}$$

where **A** is the DRF response matrix containing dipole-dipole interaction kernels and polarizabilities. To account for mutual solute-solvent polarization, the QM Hamiltonian is modified by the solvent operator $\hat{H}_{\mathrm{QM/MM}}$: [61]

$$\hat{H}_{\mathrm{QM/MM}} = \sum_i \sum_k \frac{q_k}{|\mathbf{r}_k - \mathbf{r}_i|} - \sum_i \sum_k \boldsymbol{\mu}_k^{\mathrm{ind}}(\rho_{\mathrm{QM}}) \frac{\mathbf{r}_k - \mathbf{r}_i}{|\mathbf{r}_i - \mathbf{r}_k|^3}, \quad (3)$$

where the first term represents the potential generated at position $\mathbf{r}_i$ by the fixed charges q_k associated with each MM atom, while the second term describes the electric field generated by the solvent-induced dipoles $\boldsymbol{\mu}_k^{\mathrm{ind}}$ at position $\mathbf{r}_i$, which are functions of the state of interest. By including these terms, the presence of the external environment influences the electronic QM density, and, at the same time, the induced dipoles depend on the QM density, introducing a non-linear contribution to the Kohn-Sham equations. Further information about this model can be found in Ref. 61.

The Time-Dependent Density Functional Theory (TDDFT) formalism, in its linear response formulation, is employed to calculate the QM/DRF excitation energies and spectra, as commonly reported in the literature for various QM/MM models. [50,52,62,85,86] The TDDFT equations are modified by explicit contributions of the solvent model, [62] dependent on the perturbed solvent dipoles adjusted to the transition density.

We finally note that the protocol above is general enough to be applied to deep-eutectic solvents of any nature and other polarizable QM/MM models, such as QM/FQ [51,53,58] or QM/FQFμ [49,52,87,88], pending a reliable parametrization is available.

3. Experimental procedure

All employed reagents and solvents have been used without further purifications, where not differently mentioned. Ethylene glycol (EG), choline chloride (ChCl), and hydrochloric acid were purchased from Alfa Aesar (Thermo Fisher –Germany). Gallic acid (GAL), *p*-coumaric acid (COU), syringic acid (SYR), vanillic acid (VAN), and 2-hydroxymethylfurfural (HMF) were purchased from TCI Chemicals - Europe N.V. and caffeic acid (CAF) from Merck Life Science S.r.l.–Germany. The DES used for this study is prepared by mixing 1 equivalent of ChCl with 3 equivalents of EG (ChCl:3EG). The mixture is stirred at 80 °C for 4 hours and subsequently dried under vacuum at the rotary evaporator at 80 °C for 2 h. UV-Vis absorption spectra are recorded on a Cary 300 Agilent Spectrometer (frame aperture: 2 nm, lamp change at 350 nm). Two main series of samples are prepared by dissolving the selected polyphenols (and HMF) in ChCl:3EG and water (pH = 2, by addition of hydrochloric acid). GAL, COU, SYR, and VAN spectra are recorded at a concentration of $2.5 \cdot 10^{-5}$ M, CAF and HMF spectra are recorded at a concentration of $3 \cdot 10^{-5}$ M.

4. Computational details

This study considers HMF and five polyphenols COU, CAF, VAN, SYR, and GAL (see Fig. 1 for their molecular structures) dissolved in water, DES (ChCl:3EG), and water/DES mixture (only for VAN).

Classical MD simulations are performed for each solute in the selected solvents by using the GROMACS package. [89] OPLS force field (FF) [90] is employed to describe intramolecular interactions of HMF, VAN, SYR, and COU. GAFF force field is employed for GAL and CAF because OPLS FF cannot properly describe the rotation of adjacent –OH groups (see Fig. S1 in the Supplementary Material – SM). The TIP3P [91] FF is used to describe water molecules in all instances, while Van der Waals and charge parameters for DES are taken from Ref. 36. To refine electrostatic interactions, RESP charges [92] are computed at B3LYP/6-31+g(d,p) level of theory for each solute. Lennard–Jones terms are calculated using the Lorentz–Berthelot mixing rules, and intramolecular interactions between atom pairs separated by up to three bonds are excluded. The particle–mesh Ewald (PME) method with a grid spacing of 0.16 Å and a spline interpolation of fourth order is employed for treating electrostatic interactions. [93] For aqueous solutions, a single solute molecule is dissolved in a cubic box containing at least 2900 water molecules, while for DES solutions, a single solute molecule is dissolved in a box containing 300 EG and 100 ChCl molecules. For water/DES mixtures, we dissolve VAN in three solutions with different water/DES ratios (25, 50, 75 mol%). Each molecular system is first optimized by applying the steepest descent minimization procedure, followed by NVT equilibration where each system is heated to 298.15 K using a velocity-rescaling [94] method with an integration time step of 1 fs for a 50 ps. Then, a 100 ps NPT run is performed using the Parrinello-Rahman barostat and a coupling constant of 1 ps to achieve a uniform distribution of molecules in the box. Finally, 5 ns long MD runs are performed for each MD setup in the NVT ensemble, with 1 fs time step. 200 uncorrelated snapshots are extracted from the MD trajectories of each solution and cut in a spherical shape of 18Å radius. The droplet radius is chosen by performing a preliminary analysis of a snapshot of VAN (see Fig. S2 in the SM). 200 snapshots guarantee the convergence of the computed spectra (vide infra). On each snapshot, TDDFT QM/DRF calculations are performed at the CAMY-B3LYP/DZP level of theory by considering 10 excited states. The raw data are convoluted with Gaussian functions using a full width at half maximum (FWHM) of 0.1 eV. The resulting properties are then averaged to generate the final spectra. The SCM AMS program package [95] is used for all QM/DRF calculations.

5. Results and discussion

The conformational variability of the various organic probes dissolved in water, water/DES, and DES solutions as obtained from the MD trajectories, and physicochemical insights are provided by analyzing the solvent patterns. Then, the computed QM/DRF UV/Vis absorption spectra of all systems are presented and compared with our experimental measurements.

5.1. Conformational analysis

Conformational analysis is carried out by studying the distributions of the main dihedral angles of each molecule as extracted from MD runs. Dihedral distribution functions (DDFs) for each molecule dissolved in DES are graphically depicted in Fig. 2 (DDFs in water are given in Fig. S3 in the SM). At first, the three dihedral angles of HMF (δ_1, δ_2, and δ_3, see Fig. 2(a)) are examined: δ_1 DDF centers at about 0 degrees, δ_2 at about 180 degrees, while δ_3 presents a wider range of values, with a distribution centered at 60 and -60 degrees. This reflects the high mobility of the –OH group. Then, COU and CAF acids, grouped due to their comparable molecular structures (see Fig. 2(b,c)) are analyzed. CAF differs from COU for the additional hydroxyl group attached to the benzene ring only. In this case, three dihedral angles for COU (δ_1, δ_2, and δ_3) are considered, while for CAF, a fourth dihedral angle (δ_4), related to the additional hydroxyl group, is analyzed. For both acids, δ_1 and δ_2 DDFs exhibit two main peaks at approximately 0 and 180 degrees. The same is valid for COU δ_3 DDF, while CAF δ_3 and δ_4 DDFs are centred at approximately 180 and 0 degrees, respectively. This suggests that the two hydroxyl groups are involved in intramolecular hydrogen bonding (HB). VAN, SYR, and GAL DDFs (see Fig. 2(d-f)), which are structurally similar (see Fig. 1), are analyzed. They only differ in the type (–OH vs. –OCH_3) and the number of functional groups bonded to the benzene ring. Specifically, VAN features a single hydroxyl and one methoxy group, SYR boasts one hydroxyl and a pair of methoxy groups, and three hydroxyl groups characterize GAL. The conformational flexibility of VAN and SYR is analyzed in terms of two dihedral angles (δ_1 and δ_2, see Fig. 2(d-e)). VAN δ_1 and δ_2 DDFs are centered at about 180 and 0 degrees, respectively, implying that the –OH group preferentially forms an intramolecular HB with the methoxy group. SYR δ_1 DDF has a main peak at 180 degrees, while δ_2 DDF presents two peaks at around

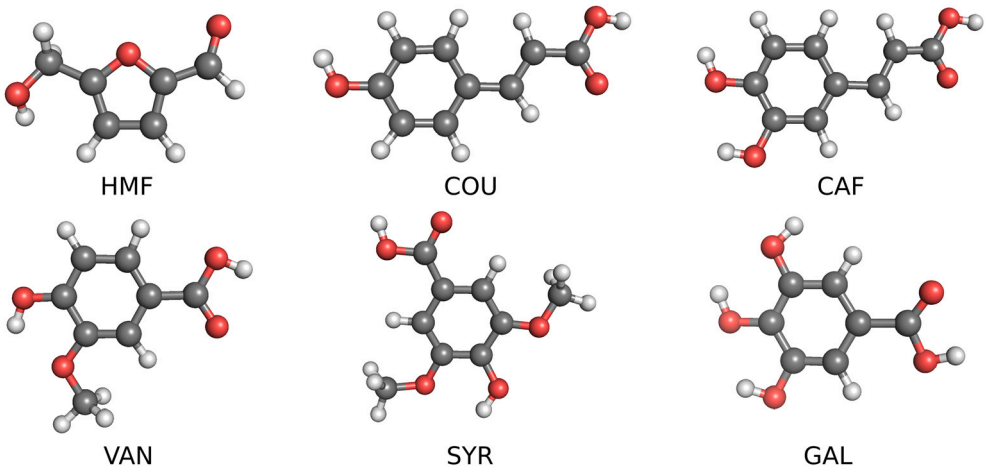

Fig. 1. Representative structures of the main conformer for the six investigated molecules: 2-hydroxymethylfurfural (HMF), p-coumaric acid (COU), caffeic acid (CAF), vanillic acid (VAN), syringic acid (SYR), and gallic acid (GAL).

0 and 180 degrees, reflecting the higher mobility of the –OH group, which, however, is involved in an intramolecular HB. For GAL, instead, we considered four dihedral angles (δ_1, δ_2, δ_3 and δ_4 see Fig. 2(f)). δ_1 assumes values around 0 degrees, while δ_2, δ_3, and δ_4, which are associated with the three hydroxyl groups, are distributed around 0 and 180 degrees, showing once again a preferential intramolecular HB, as also reported in the literature. [96]

The conformational analysis performed in DES is also valid for aqueous solution (see Fig. S3 in the SM). The main differences are reported for SYR and GAL δ_1 DDF, centered at about 0 degrees in water. The different physicochemical properties of the two solvents have a considerable impact on the time evolution of the studied dihedral angles. The fluctuations in time between 0 and 180 degrees of COU δ_3, CAF δ_3 and δ_4, and GAL δ_2, δ_3 and δ_4 occur faster in water than in DES (see Fig. S4 in the SM), suggesting higher mobility of the OH group in aqueous solution. This is not surprising and may be related to the greater mobility, associated with lower viscosity, of water molecules as compared to DES (see also Ref. 97).

5.2. Hydration pattern

The interactions of HMF and polyphenols with solvent molecules are further analyzed using radial distribution functions $g(r)$ (RDFs) and the running coordination numbers (RCNs), which indicate the number of closest solvent molecules that interact with the solutes via HB. RDFs (normalized) and RCNs for all molecules are depicted in Fig. 3, where the aqueous solution (top) and the EG component of the DES environment (bottom) are considered.

HMF RDFs and RCNs associated with the aldehyde group (O1, see Fig. 3(a)) and the hydroxyl group (O2H1, see Fig. 3(a)) are first examined. O1 RDF with water hydrogen (Hw) is characterized by a peak at about 1.9 Å, and the associated RCN indicates that two HBs are established (RCN = 1.9, see Fig. 3(a) top panel). A similar outcome is valid for O2 (RDF maximum at about 1.9 Å, RCN = 1.7), while H1 RDF shows a peak at 1.9 Å with an RCN of 1.0. Thus, the hydroxyl group is involved in three HBs with the surrounding water molecules, two via the oxygen atom and one via the hydrogen atom.

HMF O1, O2, and H1 RDFs with EG are reported in Fig. 3(a) (bottom): they all present a maximum at about 1.8/1.9 Å, similarly to the aqueous solution. However, the associated RCNs are generally lower: 0.4 (O1), 0.6 (O2) and 0.2 (H1). This is because EG molecular size is much larger than water and thus is characterized by a more significant steric hindrance. Consequently, EG cannot persistently establish an HB with HMF. In addition, an intense peak between HMF H1 and Cl can be observed at 2.4 Å with an associated RCN of 0.8 (see Fig. S5(a) in the SM). Therefore, a competing effect between Cl and EG, which decreases both RCNs, is also present. Remarkably, our simulations suggest that the Ch moiety is not involved in specific solute-solvent interactions. This observation can be explained by considering that HMF forms weaker interactions with Ch than with EG and Cl. Also, Ch has a lower concentration and a larger molecular size than EG; thus, less probably interacts with the solute.

Following, COU and CAF RDFs and RCNs are analyzed. In aqueous solution (see Fig. 3(b-c), top), the carboxylic group of both CAF and COU acids (O1H1) forms HBs with almost three solvent molecules. Specifically, O1 RDF exhibits a first peak at approximately 1.9 Å with an RCN of 1.7, while H1 RDF peaks at around 1.8 Å with an RCN of approximately 1.0. The hydroxyl groups (O2H2 for COU; O2H2 and O3H3 for CAF) are hydrogen-bonded to two solvent molecules (RCNs of H2, H3, O2, and O3 atoms are approximately 1.0). Regarding DES solutions, COU and CAF RDFs with EG are reported in Fig. 3(b-c) (bottom). Similar considerations for HMF are also valid for both molecules. While the maximum of RDFs indicates the establishment of HB interactions (~ 1.8/1.9 Å), the associated RCNs are generally lower than in water. Again, COU and CAF hydrogen atoms (H1 and H2) strongly interact with Cl (see Fig. S5(b-c) in the SM), confirming the aforementioned competition between EG and Cl.

As the last set, the interactions with water and DES of VAN, SYR, and GAL are considered by using RDFs and RCNs reported in Fig. 3(d-f) for the interactions with water (top panel) and EG (bottom panel) and Fig. S5(d-f) in the SM for the interactions with Cl. The carboxylic group of these acids (O1H1) has the same behaviour already discussed for the previous molecules, forming HBs with almost three water molecules (RDF maxima at about 1.7-1.9 Å, RCN ~ 1.6 and 1.0 for O1 and H1, respectively). The hydroxyl group O2H2 in both VAN and SYR is sterically hindered by the presence of one and two methoxy groups, respectively. Indeed, Fig. 3(d-e) shows that the distances between the hydroxyl groups and the solvent molecules are higher compared to those of the other acids (about 2.0 Å), and the associated RCNs are lower (below 1.5). The two meta hydroxyl groups (O2H2 and O4H4) establish an average of two HBs with solvent molecules in GAL. However, due to its steric hindrance, the para hydroxyl group O3H3 does not present a first solvation shell, and the reported RCN refers to the second shell. The interaction of VAN, SYR, and GAL with DES EG (refer to Fig. 3(d-f) (bottom)) is consistent with the results obtained for the other systems. HB interactions are indeed present, but the number of closest EG is again lower than in aqueous solution. The competing effect of Cl is reported for all molecules (see Fig. S5 in the SM).

Overall, all six investigated molecules strongly interact with water and DES, primarily through specific HBs. The quantity of closest water molecules to the solute is higher than the number of closest EG

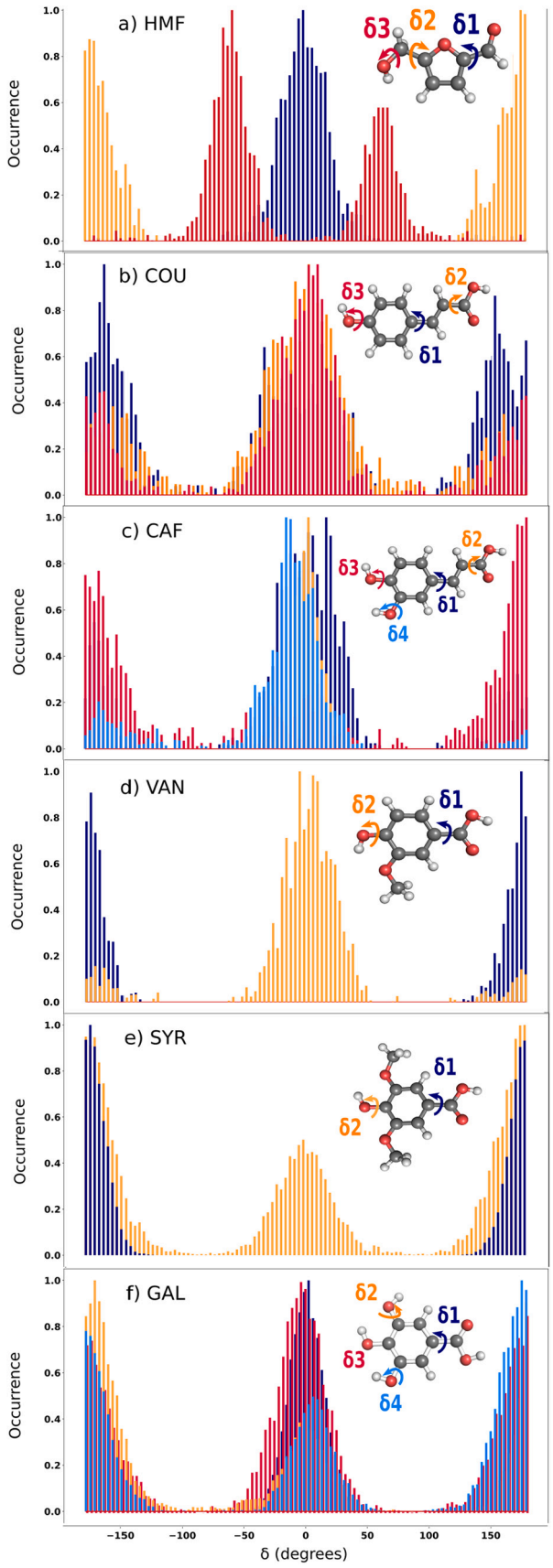

Fig. 2. Dihedral distribution functions of the six investigated molecules, as resulting from molecular dynamics (MD) simulations.

molecules for steric reasons, and in the case of DES the solute also interacts strongly with chloride ions.

5.3. Absorption spectra

This section discusses the computed absorption spectra of the six molecules in DES and aqueous solutions and their comparison with experimental data. Spectra are computed using the polarizable QM/DRF model and averaging the results on 200 uncorrelated snapshots extracted from MD trajectories. As shown in Fig. S6 in the SM, 200 snapshots are enough to reach convergence; in fact, considering additional structures does not affect the spectra. The final averaged spectra along with experimental data are shown in Fig. 4.

In Fig. 4, stick spectra as grey lines obtained directly from QM/DRF calculations on DES solutions are also reported. Excitation energies and intensities largely vary as a function of the snapshot due to the different conformations of the solute and the various distributions of DES molecules around it. This results from the phase-space sampling provided by MD simulations, which allows us to account for solvent-induced inhomogeneous band broadening. The final spectra are obtained by averaging stick spectra with a Gaussian function (FWHM = 0.1 eV). Let us discuss our findings by starting with HMF (see Fig. 4(a)). The computed spectra in both solvents exhibit a prominent peak at approximately 4.6 eV and a smaller peak at about 5.8 eV. We attribute the former to the $\pi \rightarrow \pi^*$ HOMO → LUMO transition, primarily involving the five-atom ring and the aldehyde group (see Fig. S8–9 in the SM). The peak at about 5.8 eV instead arises from multiple transitions with mixed excitations, mainly involving HOMO-2 → LUMO and HOMO-3 → LUMO excitations. It is worth noting that the computed spectra in DES and water are almost identical, reflecting their strong interactions with HMF, as highlighted by the interaction patterns discussed in the previous section. To quantify solvent effects, we performed additional QM calculations in the gas phase (see Tab. S1 in the SM). From the absorption maxima in vacuo (E_{vac}) and in solution (E_{solv}), we computed solvatochromic shifts (E_{shift}) as follows:

$$E_{shift} = E_{vac} - E_{solv} \quad (4)$$

By focusing on the lowest excitation, the resulting solvatochromic shift is 0.45 eV for both DES and water, confirming the significant impact of both solvents on HMF electronic structure.

Computed absorption spectra of COU and CAF solutions are reported in Fig. 4(b-c), together with their experimental counterparts. In both solvents, computed spectra exhibit 3 main peaks. The peak at ∼ 4.1 eV is primarily due to the $\pi \rightarrow \pi^*$ HOMO → LUMO transition (see Fig. S8–9 in the SM). This excitation involves the aromatic ring, the electron donor groups (–OH), and the electron-withdrawing group (–COOH). In addition, it is characterized by a partial charge-transfer character from the oxygen atoms bound to the benzene ring to the carboxylic group (see Fig. S8–9 in the SM). The intense peak at ∼ 5.3-5.5 eV comes from two electronic excitations (HOMO-1 → LUMO, HOMO → LUMO+1). The assignment of the third peak (∼ 5.8-6 eV) is challenging because many electronic excitations contribute to it. We can also note a small peak at ∼ 4.8 eV arising from multiple excitations, especially $\pi \rightarrow \pi^*$ HOMO-1 → LUMO. Both solvents exert a significant influence on the excitation energies, as evidenced by the DES-to-vacuo (0.36 eV for COU and 0.37 eV for CAF) and water-to-vacuo (0.39 eV for COU and 0.35 eV for CAF) solvatochromic shifts. COU and CAF spectra in both solvents are indeed very similar. This is because the two acids are characterized by a similar molecular structure (see Fig. 1), as already pointed out in the discussion of interaction patterns.

VAN, SYR, and GAL (see Fig. 4(d-f)) are now analyzed. The simulated spectra of VAN exhibit three main peaks (see Fig. 4(d)), associated with $\pi \rightarrow \pi^*$ HOMO → LUMO (∼ 4.5 eV), HOMO-1 → LUMO (∼ 5.0 eV), and HOMO → LUMO +1 (∼ 5.7 eV) transitions. SYR and GAL simulated spectra (see Fig. 4(e,f)) present two broad peaks centered at approximately 4.7 eV and between 5.7 eV (SYR) and 6.0 eV (GAL), the

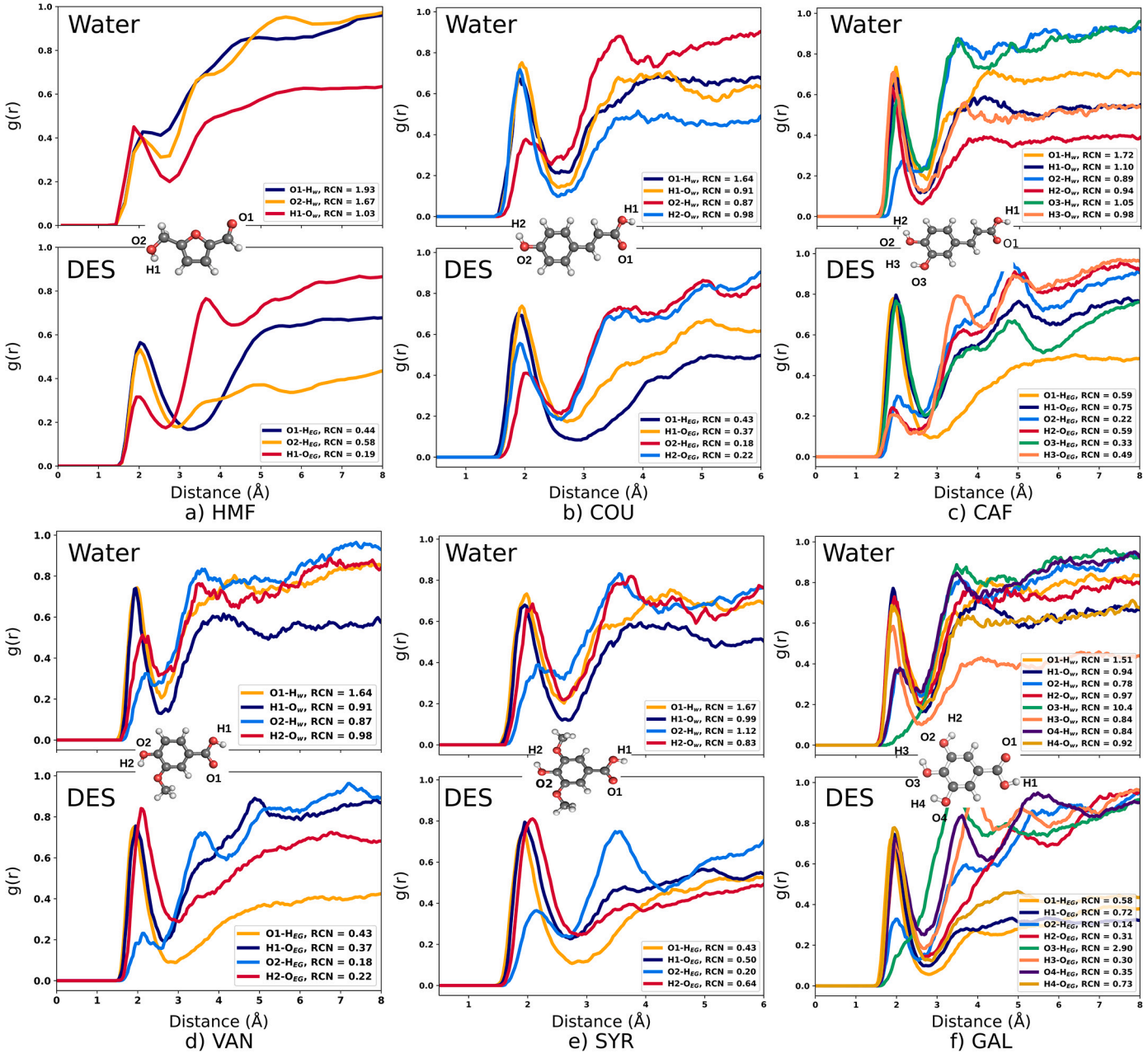

Fig. 3. Normalized Radial Distribution Functions (RDFs) and Running Coordination Numbers (RCNs) of the six investigated molecules (HMF, COU, CAF, VAN, SYR, and GAL) in water and DES.

latter being characterized by an evident shoulder. For both acids, the first peak is mainly due to the $\pi \rightarrow \pi^*$ HOMO → LUMO and secondly to the HOMO-1 → LUMO excitations. The second band is associated with the $\pi \rightarrow \pi^*$ HOMO → LUMO+1 and $\pi \rightarrow \pi^*$ HOMO-1 → LUMO+1 transitions. It is worth noting that VAN spectra differ from those of SYR and GAL despite the discussed structural similarities. This discrepancy can be explained by the fact that VAN has a free hydroxyl group attached to the benzene ring, drastically affecting its electronic properties (see also MOs in Fig. S8–9 in the SM). On the other hand, SYR and GAL spectra are similar because they both have three substituents attached to the benzene ring, which are directly involved in the electronic excitations (see S8–9 in the SM). For GAL, we report minor variations in the calculated spectra of the moiety dissolved in water and DES. The absorption spectrum in DES is slightly shifted towards lower energy than in aqueous solution. Due to the nature of the involved transitions, this indicates stronger solute-solvent interactions and can be rationalized by considering that GAL can establish a complex pattern of solute-solvent interactions due to the presence of the three hydroxyl groups attached to its benzene ring. Both DES and water exert a strong solvent effect on VAN, SYR, and GAL: the solvatochromic shifts are 0.32 eV (DES) and 0.37 eV (water) for VAN, 0.22 eV (DES) and 0.19 eV (water) for SYR, and 0.38 eV (DES) and 0.23 eV (water) for GAL.

The computed and experimental data were compared (see dashed lines in Fig. 4). The agreement between theory and experiments is excellent for each studied molecule, particularly concerning excitation energies and the related intensities. Remarkably, our approach can reproduce the experimental inhomogeneous band-broadening due to an effective sampling of the conformational solute-solvent phase space. Overall, experimental spectra measured in water and DES are similar for all investigated systems, although some subtle differences are noticeable for some compounds, and our approach can effectively reproduce this feature.

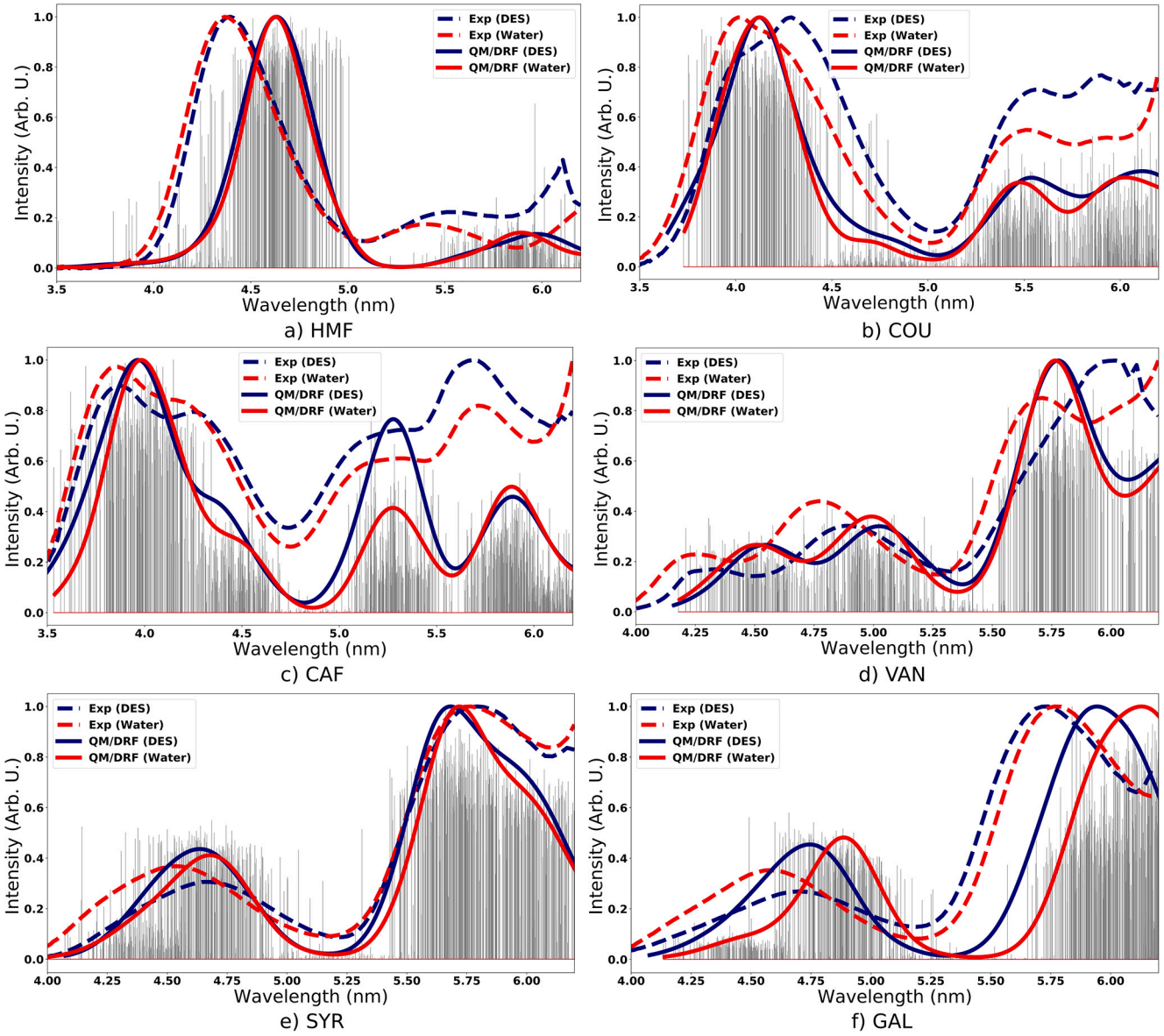

Fig. 4. Computed QM/DRF (solid) and measured (dashed) absorption spectra of HMF, COU, CAF, VAN, SYR, and GAL in water (red) and DES (blue). Raw data in DES are also shown as stick spectra (grey).

5.4. Water-DES mixtures

As mentioned earlier, due to its dual action of HBD and HBA, water may cause both beneficial or detrimental effects when present in DESs. Indeed, it has been reported before that the addition of water to DESs up to roughly 40 mol% determines the reduction of viscosity which is often exploited for favouring mass transfer at least with acid- or sugar-based DESs. Several works on extraction processes either of added value compounds from agricultural waste, [98–100] or of lignocellulose components during biomass fractionation, [101–103] or on organic reactions, [15,104] took advantage of this water-promoted effect. It is also worth mentioning that complete dehydration is rarely achieved in realistic experimental solutions when dealing with the vast majority of hydrophilic DESs. On the other hand, above a certain quantity, which is to be defined for each specific DES, water can determine the transition from water-in-DES systems to DES-in-water and finally to aqueous electrolyte-like solutions, which means DES structure disaggregation. Since the paramount work by Edler et al., [66] a great deal of attention has been devoted to understanding the effect of water on DESs using theoretic and spectroscopic techniques. [105–108] The previous section has focused on pure water or DES solutions, however the fully atomistic nature of the computational protocol here proposed permits us to describe the intermediate situations. To showcase such versatility, the case of VAN dissolved in water-DES mixtures with varying water concentrations (25, 50, and 75 mol%) was considered. The VAN conformational freedom in the selected mixtures in terms of DDFs is first analyzed (see Fig. S7 in SM). δ_1 and δ_2 DDFs are centered at about 180 and 0 degrees, respectively, similarly to the pure DES solution. Notably, there are no significant variations by varying the water-DES percentages. Thus, in water-DES mixtures, the –OH group preferentially forms intramolecular HB with the methoxy group. VAN interactions with the three water-DES mixtures are analyzed in terms of RDF and RCN, which are reported in Fig. 5(b). Regarding the carboxylic group (O1H1), both O1 and H1 exhibit a peak at about 1.8 Å with water and EG. Upon an incremental change from 25% to 75% molar percentage of water, the RCNs of O1 and H1 with EG decrease (from 0.49 to 0.28 for O1 and from 0.38 to 0.21 for H1), while those with water increase (from 0.27 to 1.02 for O1 and from 0.14 to 0.62 for H1).

In the 75 mol% solution, VAN forms almost 2 HBs with water molecules, as expected due to the high water concentration. Similar

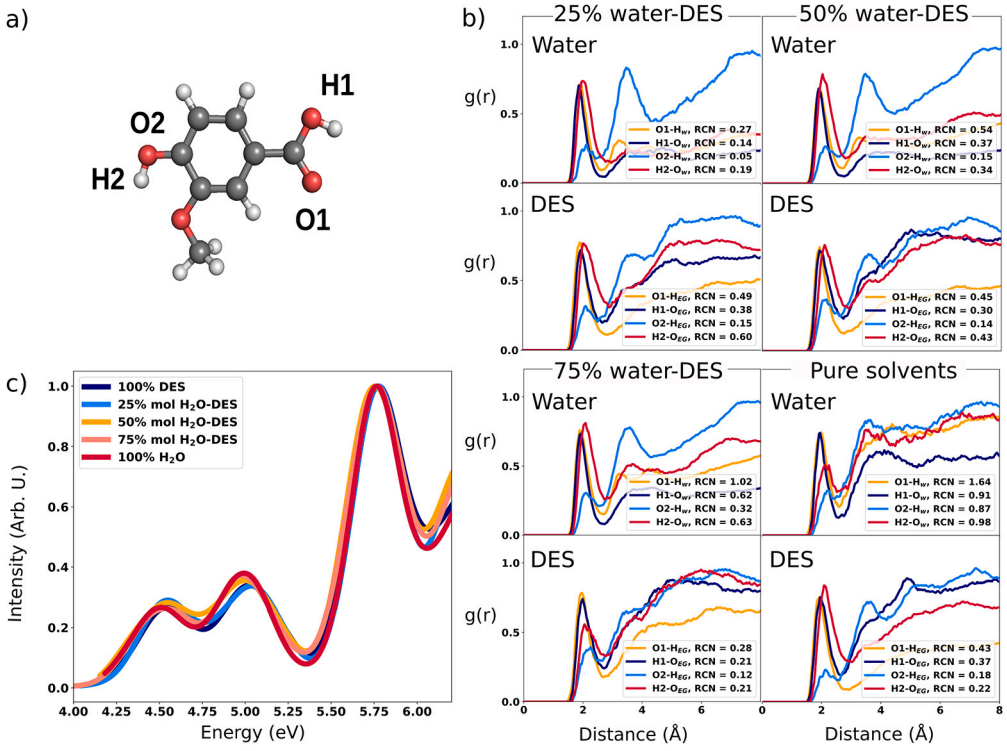

Fig. 5. VAN in water-DES mixtures at different molar percentages of water (25%, 50% and 75%) a. VAN molecular structure with atom labels, b. Normalized Radial Distribution Functions (RDFs) and Running Coordination Numbers (RCNs) and c. QM/DRF absorption spectra.

observations apply to the hydroxyl group (O2H2). When the molar percentage of water ranges between 25 mol% and 75 mol%, there is a decrease in the RCNs of O2 and H2 with EG, from 0.15 to 0.12 for O2 and from 0.60 to 0.21 for H1, respectively. Conversely, RCNs increase when water content increases, from 0.05 to 0.32 for O1 and from 0.19 to 0.63 for H1. These findings are reasonable, as the number of interactions with water increases with increasing concentration and decreases with decreasing concentration. In particular, the values reported for 25 mol% concentration closely correspond to the solvation condition of pure DES, whereas the values noticed at a concentration of 75 mol% closely correspond to the condition observed in pure water. It has been determined before that the switch from the DES to DES components in water occurred when the percentage of this latter was above 83 mol% for ChCl:urea 1:2. Although for a different DES system, the results here obtained are in line with previous findings. The VAN absorption spectra as dissolved in water-DES mixtures are reported in Fig. 5(c). Similarly to the discussed results in Fig. 4(d), absorption spectra present three main peaks, at 4.5 eV, 5.0 eV, and 5.8 eV, independently of the water molar concentration. As expected, we observe that the 25 mol% water solution spectrum better resembles that of VAN in pure DES, while the 50 mol% and 75 mol% water spectra approach that of VAN in pure aqueous solution. Therefore, the proposed protocol provides an unprecedented insight into the DES-water interactions from the solute perspective which may help in understanding the water tolerance as a function of the solute.

6. Conclusion and future perspectives

This study proposes a computational protocol to simulate the absorption properties of molecules dissolved in DES and DES/water mixtures. Our method combines classical MD simulations for sampling the solute–solvent phase space with a fully atomistic polarizable QM/MM approach to describe the electronic structure of the solvated systems. The resulting method effectively captures solute-solvent interactions, thereby modelling solvent effects on absorption properties. Indeed, the atomistic nature of the approach is crucial to describe the solute-solvent interaction patterns accurately and to accurately model the effect of solute-solvent interactions on the calculation of electronic properties. The potentialities, robustness, and versatility of the method are demonstrated by simulating absorption spectra of selected systems dissolved in water, pure DES, and water-DES mixtures.

Our analysis shows that the selected molecules strongly interact with DES. Despite this, a significant reduction in the number of solvent molecules close to the solutes is observed in DES in comparison with the same solutes dissolved in water. This is mainly due to steric factors resulting from the larger size of the DES components compared to water molecules. However, computed absorption spectra in both water and DES generally show high similarity. This is perfectly in agreement with experimental data, thus highlighting the robustness and reliability of our computational protocol.

This first work paves the way for an extensive application of the protocol to various kinds of systems dissolved in DES, also of different chemical composition than that here investigated, and even biopolymers considering the potential of these media in biomass processing. In addition, our protocol could be applied to the prediction of solvatochromic parameters of new DESs or how they may change as a function of the HBA-HBD molar ratio and/or amount of water. Such investigation would otherwise require time-consuming experiments. [109] Furthermore, our protocol could help determine the amount of water tolerated by a DES of whatever composition from the perspective of the solute, providing a unique guide for researchers in tailoring the most suitable DES system for the application of interest. The analysis of the DES behaviour with incremental amounts of water from the inside, i.e. from the solute viewpoint, had not been reported previous to this study. It thus represents a substantial step towards real case scenarios, although further investigations are needed especially in the low water amount range (below 25 mol%).

CRediT authorship contribution statement

Chiara Sepali: Software, Investigation, Formal analysis, Data curation, Conceptualization, Writing – original draft. **Sulejman Skoko:**

Investigation, Formal analysis, Data curation. **Luca Guglielmero:** Writing – original draft, Validation, Investigation, Formal analysis, Data curation. **Tommaso Giovannini:** Writing – review & editing, Software. **Andrea Mezzetta:** Validation, Investigation. **Felicia D'Andrea:** Validation. **Christian Silvio Pomelli:** Validation, Conceptualization. **Lorenzo Guazzelli:** Writing – review & editing, Supervision, Resources, Funding acquisition, Conceptualization. **Chiara Cappelli:** Writing – review & editing, Supervision, Software, Resources, Methodology, Funding acquisition, Conceptualization.

Declaration of competing interest

The authors declare that they have no known competing financial interests or personal relationships that could have appeared to influence the work reported in this paper.

Data availability

Data will be made available on request.

Acknowledgements

This work has been funded by European Union – Next Generation EU in the framework of the PRIN 2022 SEED4GREEN - Code 20223W4RT.

CC acknowledges the support of the European Union by the Next Generation EU project ECS00000017 'Ecosistema dell'Innovazione' Tuscany Health Ecosystem (THE, PNRR, Spoke 4: Nanotechnologies for diagnosis and therapy). We gratefully acknowledge the Center for High-Performance Computing (CHPC) at SNS for providing the computational infrastructure.

Appendix A. Supplementary material

Supplementary material related to this article can be found online at https://doi.org/10.1016/j.molliq.2024.124326.

References

[1] C.J. Clarke, W.-C. Tu, O. Levers, A. Brohl, J.P. Hallett, Green and sustainable solvents in chemical processes, Chem. Rev. 118 (2018) 747–800.
[2] V. Hessel, N.N. Tran, M.R. Asrami, Q.D. Tran, N.V.D. Long, M. Escribà-Gelonch, J.O. Tejada, S. Linke, K. Sundmacher, Sustainability of green solvents–review and perspective, Green Chem. 24 (2022) 410–437.
[3] A.P. Abbott, G. Capper, D.L. Davies, H.L. Munro, R.K. Rasheed, V. Tambyrajah, Preparation of novel, moisture-stable, Lewis-acidic ionic liquids containing quaternary ammonium salts with functional side chains, Chem. Commun. (2001) 2010–2011.
[4] A.P. Abbott, G. Capper, D.L. Davies, R.K. Rasheed, V. Tambyrajah, Novel solvent properties of choline chloride/urea mixtures, Chem. Commun. (2003) 70–71.
[5] T.A. Hopkins, L. VandenElzen, B.P. Nelson, V. Vaid, J. Brickley, P. Ariza, G. Whitacre, I. Patel, O. Gooch, M. Bechman, et al., Chiral solvent discovery: exploring chiral eutectic mixtures and deep eutectic solvents, Ind. Eng. Chem. Res. 62 (2023) 1606–1613.
[6] M.A. Martins, S.P. Pinho, J.A. Coutinho, Insights into the nature of eutectic and deep eutectic mixtures, J. Solution Chem. 48 (2019) 962–982.
[7] C. Velez, O. Acevedo, Simulation of deep eutectic solvents: progress to promises, Wiley Interdiscip. Rev. Comput. Mol. Sci. 12 (2022) e1598.
[8] A. Mero, S. Koutsoumpos, P. Giannios, I. Stavrakas, K. Moutzouris, A. Mezzetta, L. Guazzelli, Comparison of physicochemical and thermal properties of choline chloride and betaine-based deep eutectic solvents: the influence of hydrogen bond acceptor and hydrogen bond donor nature and their molar ratios, J. Mol. Liq. 377 (2023) 121563.
[9] T. El Achkar, H. Greige-Gerges, S. Fourmentin, Basics and properties of deep eutectic solvents: a review, Environ. Chem. Lett. 19 (2021) 3397–3408.
[10] B.B. Hansen, S. Spittle, B. Chen, D. Poe, Y. Zhang, J.M. Klein, A. Horton, L. Adhikari, T. Zelovich, B.W. Doherty, et al., Deep eutectic solvents: a review of fundamentals and applications, Chem. Rev. 121 (2020) 1232–1285.
[11] S. Kaur, M. Kumari, H.K. Kashyap, Microstructure of deep eutectic solvents: current understanding and challenges, J. Phys. Chem. B 124 (2020) 10601–10616.
[12] E.L. Smith, A.P. Abbott, K.S. Ryder, Deep eutectic solvents (DESs) and their applications, Chem. Rev. 114 (2014) 11060–11082.
[13] A. Paiva, R. Craveiro, I. Aroso, M. Martins, R.L. Reis, A.R.C. Duarte, Natural deep eutectic solvents–solvents for the 21st century, ACS Sustain. Chem. Eng. 2 (2014) 1063–1071.
[14] B. Tang, K.H. Row, Recent developments in deep eutectic solvents in chemical sciences, Monatsh. Chem. 144 (2013) 1427–1454.
[15] M.D. Nolan, A. Mezzetta, L. Guazzelli, E.M. Scanlan, Radical-mediated thiol–ene 'click' reactions in deep eutectic solvents for bioconjugation, Green Chem. 24 (2022) 1456–1462.
[16] A.F. Quivelli, F.V. Rossi, P. Vitale, J. Garcia-Alvarez, F.M. Perna, V. Capriati, Sustainable and scalable two-step synthesis of thenfadil and some analogs in deep eutectic solvents: from laboratory to industry, ACS Sustain. Chem. Eng. 10 (2022) 4065–4072.
[17] R.A. Sheldon, J.M. Woodley, Role of biocatalysis in sustainable chemistry, Chem. Rev. 118 (2018) 801–838.
[18] N.H. Silva, E.S. Morais, C.S. Freire, M.G. Freire, A.J. Silvestre, Extraction of high value triterpenic acids from eucalyptus globulus biomass using hydrophobic deep eutectic solvents, Molecules 25 (2020) 210.
[19] C. Vieira, S. Rebocho, R. Craveiro, A. Paiva, A.R.C. Duarte, Selective extraction and stabilization of bioactive compounds from rosemary leaves using a biphasic NADES, Front. Chem. 10 (2022).
[20] A. Ali Redha, Review on extraction of phenolic compounds from natural sources using green deep eutectic solvents, J. Agric. Food Chem. 69 (2021) 878–912.
[21] X. Li, K.H. Row, Development of deep eutectic solvents applied in extraction and separation, J. Sep. Sci. 39 (2016) 3505–3520.
[22] F.A. Vicente, M. Huš, B. Likozar, U. Novak, Chitin deacetylation using deep eutectic solvents: ab initio-supported process optimization, ACS Sustain. Chem. Eng. 9 (2021) 3874–3886.
[23] L. Hladnik, F.A. Vicente, U. Novak, M. Grilc, B. Likozar, Solubility assessment of lignin monomeric compounds and organosolv lignin in deep eutectic solvents using in situ Fourier-transform infrared spectroscopy, Ind. Crop. Prod. 164 (2021) 113359.
[24] A.D. Olugbemide, A. Oberlintner, U. Novak, B. Likozar, Lignocellulosic corn stover biomass pre-treatment by deep eutectic solvents (DES) for biomethane production process by bioresource anaerobic digestion, Sustainability 13 (2021) 10504.
[25] M. Vieira Sanches, R. Freitas, M. Oliva, A. Mero, L. De Marchi, A. Cuccaro, G. Fumagalli, A. Mezzetta, G. Colombo Dugoni, M. Ferro, et al., Are natural deep eutectic solvents always a sustainable option? A bioassay-based study, Environ. Sci. Pollut. Res. 30 (2023) 17268–17279.
[26] A. Brzęczek-Szafran, A. Siewniak, A. Chrobok, Assessment of green chemistry metrics for carbon dioxide fixation into cyclic carbonates using eutectic mixtures as catalyst: comprehensive evaluation on the example of a tannic acid-derived system, ACS Sustain. Chem. Eng. 11 (2023) 11415–11423.
[27] J. Afonso, A. Mezzetta, I. Marrucho, L. Guazzelli, History repeats itself again: will the mistakes of the past for ILs be repeated for DESs? From being considered ionic liquids to becoming their alternative: the unbalanced turn of deep eutectic solvents, Green Chem. 25 (2023) 59–105.
[28] A. Bjelić, B. Hočevar, M. Grilc, U. Novak, B. Likozar, A review of sustainable lignocellulose biorefining applying (natural) deep eutectic solvents (DESs) for separations, catalysis and enzymatic biotransformation processes, Rev. Chem. Eng. 38 (2022) 243–272.
[29] K.H. Kim, A. Eudes, K. Jeong, C.G. Yoo, C.S. Kim, A. Ragauskas, Integration of renewable deep eutectic solvents with engineered biomass to achieve a closed-loop biorefinery, Proc. Natl. Acad. Sci. USA 116 (2019) 13816–13824.
[30] L. Soh, M.J. Eckelman, Green solvents in biomass processing, ACS Sustain. Chem. Eng. 4 (2016) 5821–5837.
[31] D. Rente, M.C. Bubalo, M. Panić, A. Paiva, B. Caprin, I.R. Redovniković, A.R.C. Duarte, Review of deep eutectic systems from laboratory to industry, taking the application in the cosmetics industry as an example, J. Clean. Prod. (2022) 135147.
[32] D. Wagle, L. Adhikari, G. Baker, Computational perspectives on structure, dynamics, gas sorption, and bio-interactions in deep eutectic solvents, Fluid Phase Equilib. 448 (2017) 50–58.
[33] A. Kovács, E.C. Neyts, I. Cornet, M. Wijnants, P. Billen, Modeling the physicochemical properties of natural deep eutectic solvents, ChemSusChem 13 (2020) 3789–3804.
[34] S. Zhu, H. Li, W. Zhu, W. Jiang, C. Wang, P. Wu, Q. Zhang, H. Li, Vibrational analysis and formation mechanism of typical deep eutectic solvents: an experimental and theoretical study, J. Mol. Graph. Model. 68 (2016) 158–175.
[35] G. García, M. Atilhan, S. Aparicio, The impact of charges in force field parameterization for molecular dynamics simulations of deep eutectic solvents, J. Mol. Liq. 211 (2015) 506–514.
[36] B. Doherty, O. Acevedo, OPLS force field for choline chloride-based deep eutectic solvents, J. Phys. Chem. B 122 (2018) 9982–9993.
[37] J.P. Bittner, L. Huang, N. Zhang, S. Kara, S. Jakobtorweihen, Comparison and validation of force fields for deep eutectic solvents in combination with water and alcohol dehydrogenase, J. Chem. Theory Comput. 17 (2021) 5322–5341.
[38] X. Zhong, C. Velez, O. Acevedo, Partial charges optimized by genetic algorithms for deep eutectic solvent simulations, J. Chem. Theory Comput. 17 (2021) 3078–3087.
[39] E.S. Ferreira, I.V. Voroshylova, C.M. Pereira, M.N. DS Cordeiro, Improved force field model for the deep eutectic solvent ethaline: reliable physicochemical properties, J. Phys. Chem. B 120 (2016) 10124–10137.

[40] S. Mainberger, M. Kindlein, F. Bezold, E. Elts, M. Minceva, H. Briesen, Deep eutectic solvent formation: a structural view using molecular dynamics simulations with classical force fields, Mol. Phys. 115 (2017) 1309–1321.
[41] K. Goloviznina, Z. Gong, A.A. Padua, The CL &Pol polarizable force field for the simulation of ionic liquids and eutectic solvents, Wiley Interdiscip. Rev. Comput. Mol. Sci. 12 (2022) e1572.
[42] K. Goloviznina, Z. Gong, M.F. Costa Gomes, A.A. Padua, Extension of the CL&Pol polarizable force field to electrolytes, protic ionic liquids, and deep eutectic solvents, J. Chem. Theory Comput. 17 (2021) 1606–1617.
[43] C. Ruß, B. König, Low melting mixtures in organic synthesis–an alternative to ionic liquids?, Green Chem. 14 (2012) 2969–2982.
[44] A.K. Dwamena, D.E. Raynie, Solvatochromic parameters of deep eutectic solvents: effect of different carboxylic acids as hydrogen bond donor, J. Chem. Eng. Data 65 (2020) 640–646.
[45] C. Florindo, A. McIntosh, T. Welton, L. Branco, I. Marrucho, A closer look into deep eutectic solvents: exploring intermolecular interactions using solvatochromic probes, Phys. Chem. Chem. Phys. 20 (2018) 206–213.
[46] F. Egidi, V. Barone, J. Bloino, C. Cappelli, Toward an accurate modeling of optical rotation for solvated systems: anharmonic vibrational contributions coupled to the polarizable continuum model, J. Chem. Theory Comput. 8 (2012) 585–597.
[47] F. Lipparini, F. Egidi, C. Cappelli, V. Barone, The optical rotation of methyloxirane in aqueous solution: a never ending story?, J. Chem. Theory Comput. 9 (2013) 1880–1884.
[48] L. Goletto, S. Gómez, J.H. Andersen, H. Koch, T. Giovannini, Linear response properties of solvated systems: a computational study, Phys. Chem. Chem. Phys. 24 (2022) 27866–27878.
[49] S. Gómez, T. Giovannini, C. Cappelli, Multiple facets of modeling electronic absorption spectra of systems in solution, ACS Phys. Chem. Au. 3 (2023) 1–16.
[50] T. Giovannini, F. Egidi, C. Cappelli, Molecular spectroscopy of aqueous solutions: a theoretical perspective, Chem. Soc. Rev. 49 (2020) 5664–5677.
[51] A. Puglisi, T. Giovannini, L. Antonov, C. Cappelli, Interplay between conformational and solvent effects in UV-visible absorption spectra: curcumin tautomers as a case study, Phys. Chem. Chem. Phys. 21 (2019) 15504–15514.
[52] T. Giovannini, R.R. Riso, M. Ambrosetti, A. Puglisi, C. Cappelli, Electronic transitions for a fully polarizable qm/mm approach based on fluctuating charges and fluctuating dipoles: linear and corrected linear response regimes, J. Chem. Phys. 151 (2019) 174104.
[53] T. Giovannini, P. Lafiosca, B. Chandramouli, V. Barone, C. Cappelli, Effective yet reliable computation of hyperfine coupling constants in solution by a QM/MM approach: interplay between electrostatics and non-electrostatic effects, J. Chem. Phys. 150 (2019) 124102.
[54] T. Giovannini, M. Olszówka, F. Egidi, J.R. Cheeseman, G. Scalmani, C. Cappelli, Polarizable embedding approach for the analytical calculation of Raman and Raman optical activity spectra of solvated systems, J. Chem. Theory Comput. 13 (2017) 4421–4435, PMID: 28767240.
[55] F. Egidi, R. Russo, I. Carnimeo, A. D'Urso, G. Mancini, C. Cappelli, The electronic circular dichroism of nicotine in aqueous solution: a test case for continuum and mixed explicit-continuum solvation approaches, J. Phys. Chem. A 119 (2015) 5396–5404, PMID: 25568940.
[56] T. Giovannini, M. Macchiagodena, M. Ambrosetti, A. Puglisi, P. Lafiosca, G. Lo Gerfo, F. Egidi, C. Cappelli, Simulating vertical excitation energies of solvated dyes: from continuum to polarizable discrete modeling, Int. J. Quant. Chem. 119 (2019) e25684.
[57] J. Tomasi, B. Mennucci, R. Cammi, Quantum mechanical continuum solvation models, Chem. Rev. 105 (2005) 2999–3094.
[58] C. Cappelli, Integrated QM/polarizable MM/continuum approaches to model chiroptical properties of strongly interacting solute–solvent systems, Int. J. Quant. Chem. 116 (2016) 1532–1542.
[59] A. Warshel, M. Levitt, Theoretical studies of enzymic reactions: dielectric, electrostatic and steric stabilization of the carbonium ion in the reaction of lysozyme, J. Mol. Biol. 103 (1976) 227–249.
[60] H.M. Senn, W. Thiel, QM/MM methods for biomolecular systems, Angew. Chem., Int. Ed. 48 (2009) 1198–1229.
[61] L. Jensen, P.T. Van Duijnen, J.G. Snijders, A discrete solvent reaction field model within density functional theory, J. Chem. Phys. 118 (2003) 514–521.
[62] L. Jensen, P.T. Van Duijnen, J.G. Snijders, A discrete solvent reaction field model for calculating molecular linear response properties in solution, J. Chem. Phys. 119 (2003) 3800–3809.
[63] J.M. Olsen, K. Aidas, J. Kongsted, Excited states in solution through polarizable embedding, J. Chem. Theory Comput. 6 (2010) 3721–3734.
[64] H. Moradi, N. Farzi, Experimental and computational assessment of the physicochemical properties of choline chloride/ethylene glycol deep eutectic solvent in 1: 2 and 1: 3 mole fractions and 298.15–398.15 K, J. Mol. Liq. 339 (2021) 116669.
[65] Y. Zhang, H. Squire, B. Gurkan, E.J. Maginn, Refined classical force field for choline chloride and ethylene glycol mixtures over wide composition range, J. Chem. Eng. Data 67 (2022) 1864–1871.
[66] O.S. Hammond, D.T. Bowron, K.J. Edler, The effect of water upon deep eutectic solvent nanostructure: an unusual transition from ionic mixture to aqueous solution, Angew. Chem., Int. Ed. 129 (2017) 9914–9917.
[67] L. Sapir, D. Harries, Restructuring a deep eutectic solvent by water: the nanostructure of hydrated choline chloride/urea, J. Chem. Theory Comput. 16 (2020) 3335–3342.
[68] N. Kumar, S. Gupta, T. Chand Yadav, V. Pruthi, P. Kumar Varadwaj, N. Goel, Extrapolation of phenolic compounds as multi-target agents against cancer and inflammation, J. Biomol. Struct. Dyn. 37 (2019) 2355–2369.
[69] W.-Y. Huang, Y.-Z. Cai, Y. Zhang, Natural phenolic compounds from medicinal herbs and dietary plants: potential use for cancer prevention, Nutr. Cancer 62 (2009) 1–20.
[70] K.W.J. Wahle, I. Brown, D. Rotondo, S.D. Heys, in: M.T. Giardi, G. Rea, B. Berra (Eds.), Bio-Farms for Nutraceuticals: Functional Food and Safety Control by Biosensors, Springer US, Boston, MA, 2010, pp. 36–51.
[71] H. Mori, K. Kawabata, N. Yoshimi, T. Tanaka, T. Murakami, T. Okada, H. Murai, Chemopreventive effects of ferulic acid on oral and rice germ on large bowel carcinogenesis, Anticancer Res. 19 (1999) 3775–3778.
[72] E. Middleton, C. Kandaswami, T.C. Theoharides, The effects of plant flavonoids on mammalian cells: implications for inflammation, heart disease, and cancer, Pharmacol. Rev. 52 (2000) 673–751.
[73] I. Medina, J. Gallardo, M.J. González, S. Lois, N. Hedges, Effect of molecular structure of phenolic families as hydroxycinnamic acids and catechins on their antioxidant effectiveness in minced fish muscle, J. Agric. Food Chem. 55 (2007) 3889–3895.
[74] B. Badhani, N. Sharma, R. Kakkar, Gallic acid: a versatile antioxidant with promising therapeutic and industrial applications, RSC Adv. 5 (2015) 27540–27557.
[75] S. Bodini, S. Manfredini, M. Epp, S. Valentini, F. Santori, Quorum sensing inhibition activity of garlic extract and p-coumaric acid, Lett. Appl. Microbiol. 49 (2009) 551–555.
[76] A. Bhattacharya, P. Sood, V. Citovsky, The roles of plant phenolics in defence and communication during agrobacterium and Rhizobium infection, Mol. Plant Pathol. 11 (2010) 705–719.
[77] S.M. Mandal, D. Chakraborty, S. Dey, Phenolic acids act as signaling molecules in plant-microbe symbioses, Plant Signal. Behav. 5 (2010) 359–368.
[78] L.D. Rocha, M.C. Monteiro, A.J. Teodoro, Anticancer properties of hydroxycinnamic acids-a review, Clin. Oncol. 1 (2012) 109–121.
[79] E. Karimi, E. Oskoueian, R. Hendra, A. Oskoueian, H.Z. Jaafar, Phenolic compounds characterization and biological activities of citrus aurantium bloom, Molecules 17 (2012) 1203–1218.
[80] T. Ozcan, A. Akpinar-Bayizit, L. Yilmaz-Ersan, B. Delikanli, Phenolics in human health, Int. J. Chem. Eng. Appl. 5 (2014) 393.
[81] N. Kumar, V. Pruthi, N. Goel, Structural thermal and quantum chemical studies of p-coumaric and caffeic acids, J. Mol. Struct. 1085 (2015) 242–248.
[82] M. Działo, J. Mierziak, U. Korzun, M. Preisner, J. Szopa, A. Kulma, The potential of plant phenolics in prevention and therapy of skin disorders, Int. J. Mol. Sci. 17 (2016) 160.
[83] O. Sytar, I. Hemmerich, M. Zivcak, C. Rauh, M. Brestic, Comparative analysis of bioactive phenolic compounds composition from 26 medicinal plants, Saudi J. Biol. Sci. 25 (2018) 631–641.
[84] R. Chirinos, I. Betalleluz-Pallardel, A. Huamán, C. Arbizu, R. Pedreschi, D. Campos, HPLC-DAD characterisation of phenolic compounds from Andean oca (Oxalis tuberosa Mol.) tubers and their contribution to the antioxidant capacity, Food Chem. 113 (2009) 1243–1251.
[85] M.E. Casida, Recent Advances in Density Functional Methods: (Part I), World Scientific, 1995, pp. 155–192.
[86] J.M.H. Olsen, J. Kongsted, Adv. Quantum Chem., vol. 61, Elsevier, 2011, pp. 107–143.
[87] T. Giovannini, A. Puglisi, M. Ambrosetti, C. Cappelli, Polarizable QM/MM approach with fluctuating charges and fluctuating dipoles: the QM/FQFμ model, J. Chem. Theory Comput. 15 (2019) 2233–2245.
[88] T. Giovannini, L. Grazioli, M. Ambrosetti, C. Cappelli, Calculation of IR spectra with a fully polarizable QM/MM approach based on fluctuating charges and fluctuating dipoles, J. Chem. Theory Comput. 15 (2019) 5495–5507, PMID: 31436976.
[89] M.J. Abraham, T. Murtola, R. Schulz, S. Páll, J.C. Smith, B. Hess, E.G.RO.MA. CS Lindahl, High performance molecular simulations through multi-level parallelism from laptops to supercomputers, SoftwareX 1 (2015) 19–25.
[90] W.L. Jorgensen, D.S. Maxwell, J. Tirado-Rives, Development and testing of the OPLS all-atom force field on conformational energetics and properties of organic liquids, J. Am. Chem. Soc. 118 (1996) 11225–11236.
[91] P. Mark, L. Nilsson, Structure and dynamics of the TIP3P, SPC, and SPC/E water models at 298 K, J. Phys. Chem. A 105 (2001) 9954–9960.
[92] C.I. Bayly, P. Cieplak, W. Cornell, P.A. Kollman, A well-behaved electrostatic potential based method using charge restraints for deriving atomic charges: the RESP model, J. Phys. Chem. 97 (1993) 10269–10280.
[93] T. Darden, D. York, L. Pedersen, Particle mesh Ewald: an Nlog (N) method for Ewald sums in large systems, J. Chem. Phys. 98 (1993) 10089–10092.
[94] G. Bussi, D. Donadio, M. Parrinello, Canonical sampling through velocity rescaling, J. Chem. Phys. 126 (2007) 014101.
[95] G.t. Te Velde, F.M. Bickelhaupt, E.J. Baerends, C. Fonseca Guerra, S.J. van Gisbergen, J.G. Snijders, T. Ziegler, Chemistry with ADF, J. Comput. Chem. 22 (2001) 931–967.

[96] C. Cappelli, B. Mennucci, S. Monti, Environmental effects on the spectroscopic properties of gallic acid: a combined classical and quantum mechanical study, J. Phys. Chem. A 109 (2005) 1933–1943.
[97] F.S. Mjalli, J. Naser, Viscosity model for choline chloride-based deep eutectic solvents, Asia-Pac. J. Chem. Eng. 10 (2015) 273–281.
[98] M. Vilková, J. Płotka-Wasylka, V. Andruch, The role of water in deep eutectic solvent-base extraction, J. Mol. Liq. 304 (2020) 112747.
[99] X. Liu, N. Fu, Q. Zhang, S. Cai, Q. Wang, D. Han, B.Tang, Green tailoring with water of choline chloride deep eutectic solvents for the extraction of polyphenols from palm samples, J. Chromatogr. Sci. 57 (2019) 272–278.
[100] Y. Dai, G.-J. Witkamp, R. Verpoorte, Y.H. Choi, Tailoring properties of natural deep eutectic solvents with water to facilitate their applications, Food Chem. 187 (2015) 14–19.
[101] M. Hu, X. Li, X. Wang, Y. Yu, Y. Liu, The dawn of aqueous deep eutectic solvents for lignin extraction, Green Chem. (2023).
[102] E.K. New, T.Y. Wu, C.B.T.L. Lee, Z.Y. Poon, Y.-L. Loow, L.Y.W. Foo, A. Procentese, L.F. Siow, W.H. Teoh, N.N.N. Daud, et al., Potential use of pure and diluted choline chloride-based deep eutectic solvent in delignification of oil palm fronds, Process Saf. Environ. Prot. 123 (2019) 190–198.
[103] Y. Wang, W.-J. Zhang, J.-Y. Yang, M.-F. Li, F. Peng, J. Bian, Efficient fractionation of woody biomass hemicelluloses using cholinium amino acids-based deep eutectic solvents and their aqueous mixtures, Bioresour. Technol. 354 (2022) 127139.
[104] N. Guajardo, P. Domínguez de María, K. Ahumada, R.A. Schrebler, R. Ramírez-Tagle, F.A. Crespo, C. Carlesi, Water as cosolvent: nonviscous deep eutectic solvents for efficient lipase-catalyzed esterifications, ChemCatChem 9 (2017) 1393–1396.
[105] R. Gera, C.J. Moll, A. Bhattacherjee, H.J. Bakker, Water-induced restructuring of the surface of a deep eutectic solvent, J. Phys. Chem. Lett. 13 (2022) 634–641.
[106] M.M. Nolasco, S.N. Pedro, C. Vilela, P.D. Vaz, P. Ribeiro-Claro, S. Rudić, S.F. Parker, C.S. Freire, M.G. Freire, A.J. Silvestre, Water in deep eutectic solvents: new insights from inelastic neutron scattering spectroscopy, Front. Phys. 10 (2022) 834571.
[107] H. Kivela, M. Salomaki, P. Vainikka, E. Makila, F. Poletti, S. Ruggeri, F. Terzi, J. Lukkari, Effect of water on a hydrophobic deep eutectic solvent, J. Phys. Chem. B 126 (2022) 513–527.
[108] S. Rozas Azcona, C. Benito, R.T. Alcalde García, M. Atilhan, S. Aparicio Martínez, et al., Insights on the water effect on deep eutectic solvents properties and structuring: the archetypical case of choline chloride+ ethylene glycol, J. Mol. Liq. 344 (2021) 117717.
[109] F. Hosseinpoor, M. Jabbari, A. Farajtabar, Spectroscopic analysis of solvatochromic properties in some deep eutectic solvents and their aqueous mixtures, Mater. Chem. Horiz. 1 (2022) 143–151.